UC Irvine
UC Irvine Previously Published Works

Title

Frequency domain photon migration in the δ-P1 approximation: Analysis of ballistic, transport, and diffuse regimes

Permalink

https://escholarship.org/uc/item/61f8s9fp

Journal

Physical Review E, 72(2)

ISSN

2470-0045

Authors

You, JS
Hayakawa, CK
Venugopalan, V

Publication Date

2005-08-01

DOI

10.1103/physreve.72.021903

Copyright Information

Peer reviewed

Frequency domain photon migration in the δ-P_1 approximation: Analysis of ballistic, transport, and diffuse regimes

J. S. You,[1,2] C. K. Hayakawa,[2] and V. Venugopalan[1,2,3,*]

[1]*Department of Biomedical Engineering, University of California, Irvine, Irvine, California 92697-2715, USA*
[2]*Laser Microbeam and Medical Program, Beckman Laser Institute, University of California, Irvine,*
Irvine, California 92697-3010, USA
[3]*Department of Chemical Engineering and Materials Science, University of California, Irvine, Irvine, California 92697-2575, USA*

The standard diffusion approximation (SDA) to the Boltzmann transport equation (BTE) is commonly used to describe radiative transport for biomedical applications of frequency-domain diffuse optical imaging and spectroscopy. Unfortunately, the SDA is unable to provide accurate radiative transport predictions on spatial scales comparable to the transport mean free path and for media in which optical scattering is not dominant over absorption. Here, we develop and demonstrate the use of the δ-P_1 approximation to provide improved radiative transport estimates in the frequency domain via the addition of a Dirac δ function to both radiance and phase function approximations. Specifically, we consider photon density wave propagation resulting from the illumination of an infinite turbid medium with an embedded, intensity-modulated, spherical light source. We examine the accuracy of the standard diffusion and δ-P_1 approximations relative to Monte Carlo simulations that provide exact solutions to the BTE. This comparison establishes the superior accuracy of the δ-P_1 approximation relative to the SDA that is most notable at distances less than 3 transport mean free paths from the source. In addition, we demonstrate that the differences in photon density wave propagation in a highly forward scattering medium ($g_1 = 0.95$) vs an isotropically scattering medium ($g_1 = 0$) provides a basis to define three spatial regimes where the light field is dominated by (a) unscattered/ballistic light, (b) minimally scattered light, and (c) diffusely scattered light. We examine the impact of optical properties, source modulation frequency, and numerical aperture of detection on the spatial extent and location of these regimes.

I. INTRODUCTION

The standard diffusion approximation (SDA) to the Boltzmann transport equation (BTE) is used extensively to model radiative transport in biological tissues [1–7]. In therapeutic applications such as photodynamic therapy, the SDA is used for quantitative light dosimetry planning [8]. In diagnostic applications such as photon migration and fluorescence spectroscopy, the SDA is utilized as the theoretical platform to characterize tissue structure and composition through the determination of optical absorption (μ_a) and reduced scattering (μ_s') coefficients. When determined at multiple wavelengths, these coefficients provide information sufficient to determine concentrations of important chromophores/fluorophores as well as to quantify tissue morphology [2,9–12]. These successes notwithstanding, it is well known that the SDA provides accurate predictions only in regions where the angular distribution of the radiance is nearly isotropic [13,14]. This limitation restricts the applicability of the SDA to media in which optical scattering dominates absorption and to locations sufficiently removed from collimated light sources and interfaces with strong mismatches in refractive index [15–17]. As a result, proper application of the SDA to mea-

surements made in biological tissues demands the use of source-detector (s-d) separations greater than several transport mean free paths $[l^* \equiv 1/(\mu_a + \mu_s')]$ and wavelengths in the red to near-infrared spectral region ($\lambda = 650–1000$ nm) where $\mu_s' \gg \mu_a$.

The use of such large s-d separations at wavelengths in the red to near-infrared spectral region results in the sampling of relatively large tissue volumes ($\gtrsim$ cm^3) and limits the spatial resolution with which optical methods based on the SDA can measure and image heterogeneous tissue volumes [1]. While no experimental barriers prevent the use of s-d separations on the order of a transport mean free path ($r \lesssim l^*$) to provide sampling of small tissue volumes ($\sim$ mm^3) [18,19], their use leads to the collection of photons that experience a relatively small number of scattering events and whose distribution of propagation directions is not fully randomized. In fact, it is the asymmetric and structured nature of the angular radiance distribution that contains detailed information regarding the cellular and extra-cellular scatterers that interact with the photons during their migration from source to detector [20,21]. Thus, the use of small s-d separations provides an opportunity to extract detailed information regarding tissue morphology at various tissue depths. This has been borne out by recent work in which measurements performed at small s-d separations have been shown to be relevant to early stage detection of dysplastic epithelia, identification of margins between normal and cancerous tissues, and superficial *in vivo* imaging in animal models [18,22–25]. Interestingly, the highly asymmetric an-

─────────
*Author to whom correspondence should be addressed at Department of Chemical Engineering and Materials Science, University of California, Irvine, Irvine, CA 92697-2575. FAX: (949) 824-2541. Email address: vvenugop@uci.edu

gular light distributions present at small s-d separations is also a characteristic of radiative transport in media of moderate and low transport albedo. Thus a properly constructed radiative transport model that accommodates light fields possessing a significant degree of angular asymmetry may also provide an analytic framework capable of modeling radiative transport in media where optical absorption is comparable to or even greater than scattering. This would enable the use of wavelengths outside the "diagnostic window" of λ =650–1000 nm to provide quantitative measurement of chromophores whose main absorption features lie outside this spectral region.

Our objective is to develop an improved radiative transport model that retains the relative simplicity of the SDA but whose accuracy is preserved when applied to smaller spatial scales and media of moderate or low albedo. Ideally, this model should provide analytic expressions that are amenable to rapid computation. The principal approaches that can be taken to improve the SDA fall into three categories: (a) introduction of higher-order terms in the spherical harmonics expansion of the radiance and single-scattering phase function; (b) implementation of a more accurate mathematical description of directional photon sources; and (c) modification of time-varying terms in the governing equations to more accurately capture the ballistic nature of photon propagation. Significant work has been done in each of these categories and we will outline key results that motivate the use of the δ-P_1 approximation as a means to achieve our objectives.

Several investigators have investigated functional expansion methods to improve radiative transport predictions provided by the standard diffusion and P_1 approximations. These improvements are achieved by the approximation of the radiance and phase functions via a spherical harmonic expansion to an arbitrarily high order N [13,14,26]. However, such P_N approximations require the solution of at least $(N+1)$ coupled differential equations resulting in an involved solution procedure and complex analytic expressions. Along these lines, Dickey and co-workers [27,28] have examined radiative transport predictions given by the P_3 approximation for a steady isotropic point source embedded within a homogeneous infinite turbid medium. While this study confirmed that the P_3 approximation provides excellent predictions for the angular radiance distribution at distances several transport mean free paths from the source, the accuracy at locations proximal to the source or in media of moderate or low albedo was not examined. Using the P_3 approximation, Hull and Foster [29] developed predictions for the total fluence rate (the integral of the radiance over all 4π steradians) in infinite media and spatially resolved diffuse reflectance in semi-infinite media. The predictions provided by the P_3 approximation for the spatially-resolved reflectance were shown to be accurate at s-d separations comparable with l^* and in media with transport albedo of $a' = [\mu'_s/(\mu_a + \mu'_s)]$ $\gtrsim 0.6$. More recently, Finlay and Foster [30] applied the P_3 approximation to determine optical absorption and reduced scattering coefficients from reflectance measurements made at s-d separations comparable to l^* in tissue phantoms and in murine tumors *in vivo*. Boas and co-workers [31] used the P_3 approximation to derive frequency-domain fluence rate pre-

dictions in homogeneous infinite media and showed improved accuracy over the SDA for absorption dominant media and for source modulation frequencies up to 6 GHz for media with $\mu'_s = 1$ mm^{-1}.

While these studies have shown the P_3 approximation to provide significant improvements over the SDA for predictions of both the internal radiance and the spatially-resolved diffuse reflectance, this approach suffers from a few notable disadvantages. First, the P_3 approximation requires the solution of four coupled differential equations and results in cumbersome analytic expressions. Second, these studies have shown that the performance of the P_3 approximation degrades when considering media, such as tissue, that are characterized by a strong forward peak in their single scattering phase function resulting in large single-scattering asymmetry coefficients (i.e., $g_1 \gtrsim 0.9$) [29,31]. Given that the P_3 approximation uses a characterization of the phase function that is accurate to the third angular moment, this result appears at odds with the findings of Bevilacqua and Depeursinge [21] which showed via Monte Carlo (MC) simulations that accommodation of only the first two moments of the single scattering phase function is sufficient for accurate radiative transport predictions down to length scales of one transport mean free path. Thus the poor performance of the P_3 approximation is not due to a failure of the functional expansion method but rather due to the inadequate modeling of directional light sources that prevents the proper characterization of the transition from ballistic to diffuse light propagation.

To address this deficiency, investigators have examined how directional photon sources can be more accurately modeled within radiative transport theory. An important study by Fantini and co-workers [32] demonstrated that a modification in the analytic form of both the intensity and spatial distribution of the source term can enable the SDA to provide better predictions for frequency-domain photon migration. Specifically, the use of this modified source term eliminates the significant underprediction of the measured steady-state and modulated irradiance as well as the prediction of negative phase delays at locations proximal to the collimated source [32]. However, one shortcoming of this approach is that the proposed source functions are not derived rigorously from the BTE and the resulting governing equations provide accurate predictions only in highly scattering media, typically for $(\mu'_s/\mu_a) \gtrsim 10$.

Perhaps the most successful method to accommodate directional photon sources is the δ-Eddington (δ-E$_{N+1}$) or δ-P_N approximation. This approach, initially proposed by Joseph, Wiscombe, and Weinman [33], and more fully developed independently by Prahl [34] and by Star [35,36], is a functional expansion method that adds a Dirac δ function to the Legendre polynomial expansion used in both the radiance and phase function approximations. The addition of a Dirac δ function not only enables the precise modeling of directional photon sources but also provides an additional degree of freedom to describe the angular distributions involved in the radiative transport process. This has given rise to a significant development of the δ-P_1 and, to a lesser extent, the δ-P_3 approximation.

Specifically, Star has examined the spatial fluence rate distributions provided by the δ-P_1 and δ-P_3 approximations

within a semi-infinite medium when irradiated by a steady collimated planar source [36]. While results are given for only a single set of optical properties [$(\mu_s'/\mu_a)=13.2$, $l^*=0.26$ mm, and $g_1=0.81$], the fluence rate distributions predicted by δ-P_1 and δ-P_3 approximations provide much better accuracy than those given by the P_1 and P_3 approximations, respectively. Under similar conditions, Spott and Svaasand [37] examined the accuracy of both δ-P_1 and δ-P_3 approximations with respect to the use of various analytic source terms over a broader range of optical properties to predict both diffuse reflectance and internal fluence rate distributions. They showed vastly improved predictions for total diffuse reflectance and total fluence rate by the δ-P_1 and δ-P_3 approximations relative to the corresponding P_1 and P_3 approximations. The improvements were particularly notable in media of low albedo and at superficial depths; both of which represent conditions for which the influence of the collimated light source is prominent. While these studies provided limited information regarding the analytical expressions used to generate radiative transport predictions, the results provided persuasive evidence that adoption of δ-P_{N} approximations represent an effective approach to greatly improve radiative transport predictions at locations proximal to collimated sources. Most recently, our group provided complete analytical expressions within the δ-P_1 approximation for the internal fluence rate distribution within a planar semi-infinite medium when irradiated by steady collimated planar (1D) and Gaussian (2D, axisymmetric) laser sources with either refractive-index matched or mismatched boundaries [38]. Comparison of the δ-P_1 approximation estimates with MC simulations reveal that for planar irradiation, the δ-P_1 approximation provides fluence rate estimates accurate to ±16% over the full range of optical properties to depths of $6l^*$ and optical penetration depth estimates accurate to within ±4%.

Our group has also examined the accuracy of radiative transport predictions given by the δ-P_1 approximation through comparison to experimental measurements in infinite media. Specifically, Venugopalan and co-workers [39] provided a full development of equations governing the δ-P_1 approximation in infinite media for both steady-state and frequency-domain photon migration. Expressions providing radiative transport predictions were derived for the steady-state case only. Comparison of these predictions with measured irradiances using optical fibers that sample the angular radiance distribution over small intervals of solid angle demonstrated that the δ-P_1 approximation is particularly effective in characterizing the transition from ballistic to diffuse light propagation; especially in highly forward scattering media [39]. Specifically, the δ-P_1 approximation provides remarkably accurate radiative transport predictions over the full range of transport albedo and down to length scales approaching $l^*/4$. Moreover, the δ-P_1 approximation provides predictions that are appropriately sensitive to the single-scattering asymmetry coefficient g_1 independent of the (μ_s'/μ_a) of the medium and has been successfully used by Hayakawa and co-workers [40] for the determination of μ_a, μ_s', and g_1 from spatially-resolved irradiance measurements.

Efforts to incorporate a realistic description of the ballistic features of light propagation in turbid media within the context of the SDA and P_1 approximation has been spearheaded primarily by Durian and co-workers [41,42]. This work resulted in the development of a modified telegraphers equation and its use has proven quite accurate predicting the time-resolved transmittance and reflectance in a slab geometry for slab thicknesses down to $l^*/10$. An interesting feature of their formulation is that its accuracy is retained when considering highly absorbing media. However, while the telegraphers equation framework provides more accurate predictions for total fluence rate in the frequency domain, it does a poor job in modeling the angular variation of the light field near directional photon sources as, like the SDA, it employs the simple two-term Legendre polynomial expansion to describe both the radiance and the single-scattering phase function.

The results of these studies have led us to examine the δ-P_1 approximation for improved radiative transport predictions in the frequency domain. The δ-P_1 approximation provides a simple approach to significantly improve upon both the description of directional photon sources as well as the radiance and phase function approximations. Using this solution, we examine characteristics of the predicted frequency-domain irradiance and phase delay at various distances from an intensity-modulated point source in infinite media. These results are compared to MC simulations that provide exact (within statistical uncertainty) solutions to the BTE for a full range of transport albedo a' and single-scattering asymmetry g_1. This comparison will demonstrate that the δ-P_1 approximation provides very accurate predictions of photon density wave propagation over a wide range of optical properties and spatial regimes. These results will also provide a framework within which to examine the sensitivity of the frequency domain amplitude and phase delay to the single-scattering asymmetry. This, in turn, will provide a means to define spatial regimes within which the light field is dominated by unscattered/ballistic, multiply scattered, or diffusely scattered photons and examine how the boundaries of these spatial regimes are affected by the optical properties of the medium, the source-modulation frequency, and the numerical aperture of detection.

II. δ-P_1 MODEL FORMULATION

A. δ-P_1 approximation of the single-scattering phase function

The basis of the δ-P_1 approximation to radiative transport lies within the δ-P_1 phase function as formulated by Joseph, Wiscombe, and Weinman [33]:

$$p_{\delta\text{-}P_1}(\hat{\mathbf{\Omega}} \cdot \hat{\mathbf{\Omega}}') = \frac{1}{4\pi}\{2f\delta[1-(\hat{\mathbf{\Omega}}\cdot\hat{\mathbf{\Omega}}')]+(1-f)$$

$$\times[1+3g^*(\hat{\mathbf{\Omega}}\cdot\hat{\mathbf{\Omega}}')]\},\qquad(1)$$

where $\hat{\mathbf{\Omega}}'$ and $\hat{\mathbf{\Omega}}$ are unit vectors representing the direction of light propagation before and after scattering, respectively. In Eq. (1), f is the fraction of light scattered directly forward and is treated as unscattered/ballistic light by the δ-P_1 model. The remainder of the light $(1-f)$ is diffusely scattered according to a standard P_1 phase function with single

scattering asymmetry g^*. To determine appropriate values for f and g^*, one must choose a single-scattering phase function to approximate. In this study, we provide results for the Henyey-Greenstein (HG) phase function, as it is known to provide a reasonable approximation for optical scattering in biological tissues [43]. The HG phase function is

$$p_{HG}(\hat{\mathbf{\Omega}} \cdot \hat{\mathbf{\Omega}}') = \frac{1 - g_1^2}{4\pi[1 - 2g_1(\hat{\mathbf{\Omega}} \cdot \hat{\mathbf{\Omega}}') + g_1^2]^{3/2}}. \qquad (2)$$

Recalling that for a spatially isotropic medium, the nth moment g_n of a phase function $p(\hat{\mathbf{\Omega}} \cdot \hat{\mathbf{\Omega}}')$ is defined by

$$g_n = 2\pi \int_{-1}^{1} P_n(\hat{\mathbf{\Omega}} \cdot \hat{\mathbf{\Omega}}') p(\hat{\mathbf{\Omega}} \cdot \hat{\mathbf{\Omega}}') d(\hat{\mathbf{\Omega}} \cdot \hat{\mathbf{\Omega}}'), \qquad (3)$$

where P_n is the nth Legendre polynomial, we determine f and g^* by requiring the first two moments of the $\delta\text{-}P_1$ phase function, $g_1 = f + (1 - f)g^*$ and $g_2 = f$, to match the corresponding moments of the Henyey-Greenstein phase function which are given by $g_n = g_1^n$. This yields the following expressions for f and g^*:

$$f = g_1^2, \quad g^* = g_1/(g_1 + 1). \qquad (4)$$

For simplicity, from this point forward we refer to g_1 simply as g and all $\delta\text{-}P_1$ model results in this paper are shown for $g = 0.9$ unless noted otherwise.

B. $\delta\text{-}P_1$ approximation of the radiance

In the $\delta\text{-}P_1$ approximation the radiance is also separated into ballistic (L_b) and diffuse (L_d) components in a manner similar to the phase function:

$$L(\mathbf{r}, \hat{\mathbf{\Omega}}, t) = L_b(\mathbf{r}, \hat{\mathbf{\Omega}}, t) + L_d(\mathbf{r}, \hat{\mathbf{\Omega}}, t), \qquad (5)$$

where $\mathbf{r}$ is the position vector, $\hat{\mathbf{\Omega}}$ is the unit vector representing the direction of light propagation, and t is the time.

For the case of irradiation of an infinite medium with a single isotropic source, the ballistic radiance is given by

$$L_b(\mathbf{r}, \hat{\mathbf{\Omega}}, t) = \frac{1}{4\pi} P(\mathbf{r}, \hat{\mathbf{\Omega}}_0, t), \qquad (6)$$

where $\hat{\mathbf{\Omega}}_0$ specifies the direction of the ballistic light within the medium and $P(\mathbf{r}, \hat{\mathbf{\Omega}}_0, t)$ is the complete angular, spatial, and temporal distribution of the irradiance provided by the light source. The diffuse radiance in Eq. (5) is approximated, as in the SDA, by the sum of the first two terms in a Legendre polynomial series expansion:

$$
\begin{aligned}
L_d(\mathbf{r}, \hat{\mathbf{\Omega}}, t) &= \frac{1}{4\pi} \int_{4\pi} L_d(\mathbf{r}, \hat{\mathbf{\Omega}}, t) d\hat{\mathbf{\Omega}} \\
&+ \frac{3}{4\pi} \int_{4\pi} L_d(\mathbf{r}, \hat{\mathbf{\Omega}}', t)(\hat{\mathbf{\Omega}}' \cdot \hat{\mathbf{\Omega}}) d\hat{\mathbf{\Omega}}' \\
&= \frac{1}{4\pi} \varphi_d(\mathbf{r}, t) + \frac{3}{4\pi} \mathbf{j}(\mathbf{r}, t) \cdot \hat{\mathbf{\Omega}}, \qquad (7)
\end{aligned}
$$

where $\varphi_d(\mathbf{r}, t)$ is the diffuse fluence rate and $\mathbf{j}(\mathbf{r}, t)$ is the radiant flux. The diffuse fluence rate $\varphi_d(\mathbf{r}, t)$ represents the isotropic component of the diffuse light field while the radiant flux $\mathbf{j}(\mathbf{r}, t)$ represents the anisotropic component of the diffuse light field with an angular dependence of $\cos\theta$.

The improved accuracy offered by the $\delta\text{-}P_1$ approximation stems from the addition of the Dirac δ function to both the single-scattering phase function and radiance approximations. The δ function provides an additional degree of freedom well suited to accommodate directional photon sources and highly forward-scattering media. Thus the addition of the δ-function relieves substantially the degree of asymmetry that must be provided by the first-order term in the Legendre expansion [44].

C. $\delta\text{-}P_1$ governing equations in the frequency domain

The substitution of Eqs. (1) and (6), and (7) into the Boltzmann transport equation followed by the application of the appropriate balances in both the fluence rate and the radiant flux provides the governing equations in the $\delta\text{-}P_1$ approximation [39],

$$
\begin{aligned}
&\nabla^2 \varphi_d(\mathbf{r}, t) - 3\mu_a \mu_{tr} \varphi_d(\mathbf{r}, t) - \frac{3}{v^2} \frac{\partial^2 \varphi_d(\mathbf{r}, t)}{\partial t^2} \\
&\quad - \frac{3(\mu_a + \mu_{tr})}{v} \frac{\partial \varphi_d(\mathbf{r}, t)}{\partial t} \\
&= -3\mu_s^* \mu_{tr} P(\mathbf{r}, \hat{\mathbf{\Omega}}_0, t) + 3g^* \mu_s^* \nabla P(\mathbf{r}, \hat{\mathbf{\Omega}}_0, t) \hat{\mathbf{\Omega}}_0 \\
&\quad - \frac{3}{v^2} \frac{\partial^2 P(\mathbf{r}, \hat{\mathbf{\Omega}}_0, t)}{\partial t^2} + \frac{3(\mu_{tr} - \mu_s^*)}{v} \frac{\partial P(\mathbf{r}, \hat{\mathbf{\Omega}}_0, t)}{\partial t} \\
&\quad - \frac{3}{v} \nabla \frac{\partial}{\partial t} [\hat{\mathbf{\Omega}}_0 P(\mathbf{r}, \hat{\mathbf{\Omega}}_0, t)], \qquad (8)
\end{aligned}
$$

$$
\begin{aligned}
\mathbf{j}(\mathbf{r}, t) = \mathcal{K}^{-1} \Big\{ &-\frac{1}{3} \nabla \varphi_d(\mathbf{r}, t) + g^* \mu_s^* P(\mathbf{r}, \hat{\mathbf{\Omega}}_0, t) \hat{\mathbf{\Omega}}_0 \\
&- \frac{1}{v} \frac{\partial}{\partial t} [\hat{\mathbf{\Omega}}_0 P(\mathbf{r}, \hat{\mathbf{\Omega}}_0, t)] \Big\}, \qquad (9)
\end{aligned}
$$

where the operator $\mathcal{K} \equiv [(1/v)(\partial/\partial t) + \mu_{tr}]$ and $\mu_s^* = \mu_s(1 - f)$.

To solve these equations for an infinite medium in the frequency domain, we consider a source function $P(\mathbf{r}, \hat{\mathbf{\Omega}}, t)$ of the form

$$
\begin{aligned}
P(\mathbf{r}, \hat{\mathbf{\Omega}}, t) = &\frac{P_0 \exp[-\mu_t^*(r - r_0)]}{4\pi r^2} \delta(1 - \hat{\mathbf{\Omega}} \cdot \hat{\mathbf{r}}) \\
&\times \{1 + M \exp[-i(\omega t + \varepsilon)]\}, \qquad (10)
\end{aligned}
$$

where $i = \sqrt{-1}$ and $\mu_t^* = \mu_a + \mu_s^*$. This function represents an intensity-modulated spherical light source of radius r_0, with an average output power P_0 modulated in time at an angular frequency ω, phase offset ε, and modulation depth M. The directionality of the photon source is achieved by the term $\delta(1 - \hat{\mathbf{\Omega}} \cdot \hat{\mathbf{r}})$ that specifies the ballistic light to be emitted from the source in a direction $\hat{\mathbf{\Omega}}$ collinear with the outward-pointing radial unit vector $\hat{\mathbf{r}}$. The diffuse fluence rate can also

be separated into steady (dc) and oscillatory (ac) components:

$$\varphi_d(\boldsymbol{r},t) = \varphi_d^{dc}(\boldsymbol{r}) + \varphi_d^{ac}(\boldsymbol{r})\exp[-i(\omega t + \varepsilon)]. \quad (11)$$

In this work, we focus on the frequency-dependent (ac) component of the fluence rate. Substitution of Eqs. (10) and (11) into Eq. (8), provides the governing equation for the ac component of the diffuse fluence rate as [39]

$$\nabla^2 \varphi_d^{ac}(\boldsymbol{r}) - 3\left[\mu_a\mu_{tr} - \frac{\omega^2}{v^2} - \frac{i\omega(\mu_a + \mu_{tr})}{v}\right]\varphi_d^{ac}(\boldsymbol{r})$$

$$= -3\left[\mu_s^*(\mu_t^* + g^*\mu_a) - \frac{\omega^2}{v^2} + \frac{i\omega(\mu_{tr} + \mu_a)}{v}\right]$$

$$\times \frac{P_0 M \exp[-\mu_t^*(r-r_0)]}{4\pi r^2}, \quad (12)$$

where v is the velocity of light in the medium and $\mu_{tr} = \mu_a + \mu_s'$.

Boundary equations are provided by enforcing conservation of diffuse radiance $L_d(\boldsymbol{r},\hat{\boldsymbol{\Omega}},t)$ at $r=r_0$ and requiring $\varphi_d^{ac}(\boldsymbol{r})$ to vanish at large r. These take the mathematical form

$$\left[\varphi_d^{ac}(\boldsymbol{r}) - \left(\frac{2Av}{3v\mu_{tr} - 3i\omega}\right)\nabla\varphi_d^{ac}(\boldsymbol{r})\cdot\hat{\boldsymbol{r}}\right]\Bigg|_{r=r_0}$$

$$= \left[\frac{-2Av}{v\mu_{tr} - i\omega}\left(g^*\mu_s^* + \frac{i\omega}{v}\right)\frac{P_0 M}{4\pi r_0^2}\right]\Bigg|_{r=r_0}, \quad (13)$$

$$\varphi_d^{ac}(\boldsymbol{r})|_{r\to\infty} \to 0. \quad (14)$$

With these boundary conditions, the solution for Eq. (12) is

$$\varphi_d^{ac}(r,\omega) = \frac{3P_0 M \exp(\mu_t^* r_0)}{8\pi\mu_{eff}^{AC} r}\left\{\left[\mu_s^*(\mu_t^* + g^*\mu_a) - \frac{\omega^2}{v^2}\right.\right.$$

$$+ \frac{i\omega(\mu_{tr} + \mu_a)}{v}\right](E_1[\mu_t^* r_0 - \mu_{eff}^{ac} r_0]$$

$$- E_1[\mu_t^* r_0 + \mu_{eff}^{ac} r_0] - E_1[\mu_t^* r - \mu_{eff}^{ac} r])\exp(-\mu_{eff}^{ac} r)$$

$$+ (E_1[\mu_t^* r + \mu_{eff}^{ac} r])\exp(\mu_{eff}^{ac} r)] - \left[g^*\mu_s^* + \frac{i\omega}{v}\right]$$

$$\times\left[\frac{2\sinh(\mu_{eff}^{ac} r_0)}{r_0 \exp(\mu_t^* r_0)}\right]\exp(-\mu_{eff}^{ac} r)\right\}, \quad (15)$$

where μ_{eff}^{ac} is the frequency-dependent effective attenuation coefficient

$$\mu_{eff}^{ac} = \left[3\mu_a\mu_{tr} - \frac{3\omega^2}{v^2} - \frac{3i\omega}{v}(\mu_a + \mu_{tr})\right]^{1/2}, \quad (16)$$

and E_1 is exponential integral function defined as $E_1(z) = \int_z^\infty [\exp(-t)/t]dt$. The expression for the ac component of the radiant flux is then obtained from Eq. (9) by substituting Eqs. (10) and (11) for $\varphi_d(\boldsymbol{r},t)$ and $P(\boldsymbol{r},\hat{\boldsymbol{\Omega}},t)$, respectively,

$$\boldsymbol{j}^{ac}(r,\omega) = \frac{Av}{(v\mu_{tr} - i\omega)}\left\{[BC - E]\left(\frac{\mu_{eff}^{ac}}{r} + \frac{1}{r^2}\right)\exp(-\mu_{eff}^{ac} r)\right.$$

$$- BD\left(\frac{\mu_{eff}^{ac}}{r} - \frac{1}{r^2}\right)\exp(\mu_{eff}^{ac} r) + \frac{1}{A}\left(g^*\mu_s^* + \frac{i\omega}{v}\right)$$

$$\times\frac{P_0 M \exp[-\mu_t^*(r-r_0)]}{4\pi r^2}\right\}, \quad (17)$$

where

$$A = \frac{P_0 M \exp(\mu_t^* r_0)}{8\pi\mu_{eff}^{ac}}, \quad (18)$$

$$B = \mu_s^*(\mu_t^* + g^*\mu_a) - \frac{\omega^2}{v^2} + \frac{i\omega(\mu_{tr} + \mu_a)}{v}, \quad (19)$$

$$C = E_1[(\mu_t^* - \mu_{eff}^{ac})r_0] - E_1[(\mu_t^* + \mu_{eff}^{ac})r_0] - E_1[(\mu_t^* - \mu_{eff}^{ac})r], \quad (20)$$

$$D = E_1[(\mu_t^* + \mu_{eff}^{ac})r], \quad (21)$$

$$E = \left(g^*\mu_s^* + \frac{i\omega}{v}\right)\frac{2\sinh(\mu_{eff}^{ac} r_0)}{r_0 \exp(\mu_t^* r_0)}. \quad (22)$$

The ac component of the ballistic fluence rate $\varphi_b^{ac}(r,\omega)$ is given by

$$\varphi_b^{ac}(r,\omega) = \frac{P_0 M \exp[-\mu_t^*(r-r_0)]}{4\pi r^2}\delta(1 - \hat{\boldsymbol{\Omega}}\cdot\hat{\boldsymbol{r}})$$

$$\times\exp\left\{-i\left[\omega\left(t - \frac{r-r_0}{v}\right) + \varepsilon\right]\right\}. \quad (23)$$

The first exponential term in Eq. (23) describes the spatial variation of the source fluence rate from the spherical source of radius r_0. P_0 is the average power of the source with M being the modulation of the source intensity. The δ function term specifies that the direction of the light emitted by the source is collinear with the outward-pointing radial unit vector $\hat{\boldsymbol{r}}$. The last exponential term describes the phase accumulated by the ballistic light as it travels to an arbitrary position r at velocity v with angular modulation frequency ω and arbitrary phase offset ε.

Equations (12)–(23) provide a full characterization of photon migration in the frequency domain within the δ-P_1 approximation in infinite media. We have shown that these solutions reduce to that provided by the SDA when considering locations far from the source $(r \gg l^*)$ in media where scattering dominates absorption $(\mu_s' \gg \mu_a)$ [39]. Moreover, because $\varphi_d^{ac}(\boldsymbol{r}) \to 0$ in the limit $(\mu_s'/\mu_a) \to 0$, the construction of the ballistic fluence rate ensures that the δ-P_1 approximation reduces to Bouguer's law (aka Beer-Lambert law) in the limit of no scattering [39]. To utilize these expressions, we must realize that in most experimental situations the total fluence rate $\varphi_t(=\varphi_b + \varphi_d)$ is not detected and instead an optical fiber is used to measure the irradiance through a finite solid angle. Because the light field can possess strong angular asymmetry, the measured irradiance must include its de-
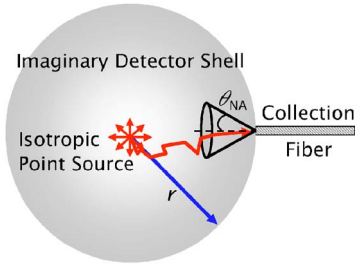
FIG. 1. (Color online) Schematic of the source-detector geometry.

pendence on the collection angle of the detector. For a collection fiber with numerical aperture NA the collection angle inside a medium with refractive index n is given by $\theta_{NA} \equiv \arcsin(NA/n)$. Here, we are interested in the characteristics of the light field measured along the radial direction from a spherical source as shown in Fig. 1. In this case the modulation-frequency dependent component of the measured irradiance is

$$I_r^{ac}(r,\omega,\theta_{NA}) = \varphi_b^{ac}(r,\omega) + \frac{1}{4}[\sin^2\theta_{NA}\varphi_d^{ac}(r,\omega)$$

$$+ 2(1-\cos^3\theta_{NA})j^{ac}(r,\omega)]. \qquad (24)$$

It is important to note that this irradiance is a complex quantity containing both amplitude and phase components.

III. MONTE CARLO SIMULATIONS

To evaluate the accuracy of the solutions given by the δ-P_1 and standard diffusion approximations to the BTE in the frequency domain, we performed Monte Carlo (MC) simulations for a point source illuminating an infinite turbid medium. The geometry employed considered the irradiance measured by an optical collection fiber of numerical aperture NA pointing directly toward an isotropic point source as illustrated in Fig. 1. In the MC simulation, a photon of unit weight is launched from the source location at a random direction sampled uniformly over 4π steradians. The photon trajectory is tracked until it reaches the boundary of the simulation domain situated at a distance $50l^*$ from the source. The intercollision distances l are sampled from the probability density function $\mu_s \exp(-\mu_s l)$ [45] and the scattering angle at each interaction point is sampled from the Henyey-Greenstein phase function [46]. Absorption is modeled by exponentially decreasing the photon weight continuously along its path, i.e., $W=\exp(-\mu_a vt)$, where the product of the photon velocity v and time of flight t provides the path length. $(1-12) \times 10^6$ photons were launched for each MC simulation.

This detection geometry possesses spherical symmetry and thus the surface of the detection fiber can be considered equivalent to an infinitesimal area on the surface of a spherical shell whose center is located at the source. The estimated frequency-domain irradiance collected by a radial detection fiber positioned at distance r is given by
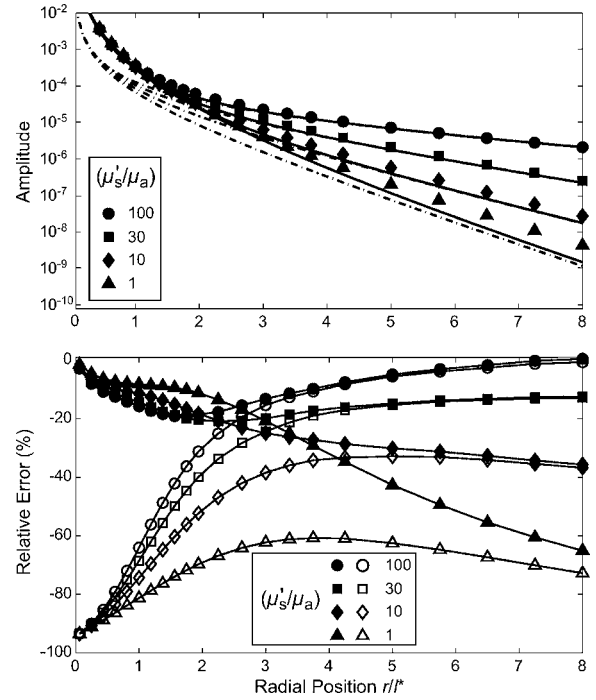

FIG. 2. (a) Photon density wave amplitude vs dimensionless radial position for turbid media with $(\mu_s'/\mu_a)=100(\bullet)$, 30 (■), 10 ($\blacklozenge$), and 1 (▲) for source modulation frequency of $f=100$ MHz and collection fiber with $NA=0.37$. Monte Carlo estimates are specified by the symbols while predictions by the δ-P_1 and standard diffusion approximation are given by the solid and dashed curves, respectively. (b) Error of the δ-P_1 and standard diffusion approximation predictions relative to the Monte Carlo estimates are specified by the solid and open symbols, respectively.

$$I_r(\omega) = \frac{1}{4\pi r^2 J}\sum_{j=1}^{J}\sum_{k=1}^{K_j}\frac{W_{j,k}\exp(-i\omega t_{j,k})}{\hat{\Omega}_{j,k}\cdot\hat{r}}, \qquad (25)$$

where J is the total number of photons launched and K_j is the total number of times the jth photon crosses the surface of a sphere of radius r centered at the origin within the acceptance angle of the detection fiber. This estimator is a limiting case of the track length estimator described in Spanier and Gelbard [47]. Calculation of the irradiance in the frequency domain avoids the quantization and sampling errors in time-domain calculations and allows direct calculations of the frequency-domain quantities from the simulations [48]. Amplitude and phase delay of the estimated complex irradiance are then calculated numerically using MATLAB (MathWorks, Natick, MA).

IV. RESULTS AND DISCUSSION

A. Effects of albedo

Figures 2(a) and 3(a) provide the variation of the amplitude and phase, respectively, of the irradiance measured by a 0.37 numerical aperture (NA) optical fiber with radial position as predicted by the δ-P_1 approximation. Results are provided for a range of optical properties spanning $100 \geqslant (\mu_s'/\mu_a) \geqslant 1$ for a point source ($r_0=0$) intensity modulated
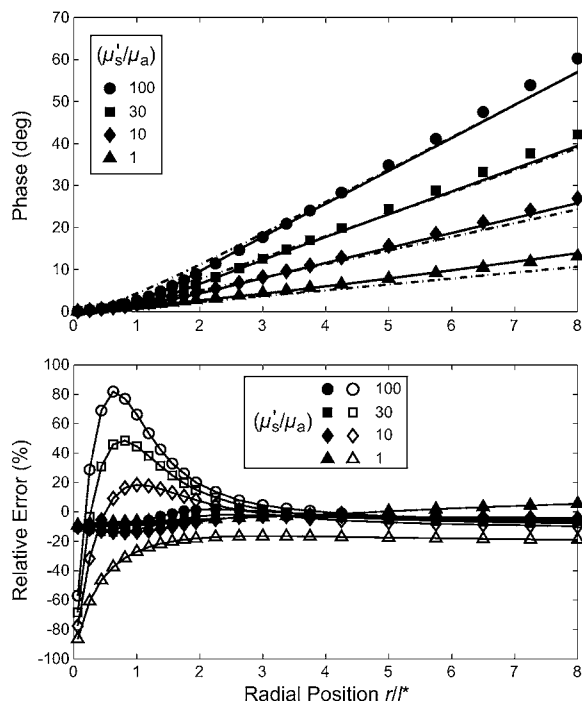
FIG. 3. (a) Photon density wave phase vs dimensionless radial position for turbid media with $(\mu_s'/\mu_a)=100(\bullet)$, 30 ($\blacksquare$), 10 ($\blacklozenge$), and 1 ($\blacktriangle$) for source modulation frequency of $f=100$ MHz and collection fiber with $NA=0.37$. Monte Carlo estimates are specified by the symbols while predictions by the δ-P_1 and standard diffusion approximation are given by the solid and dashed curves, respectively. (b) Error of the δ-P_1 and standard diffusion approximation predictions relative to the Monte Carlo estimates are specified by the solid and open symbols, respectively.

at a frequency of $f=100$ MHz. The results are plotted against a radial position normalized relative to the transport mean free path l^*. For comparison, results from the Monte Carlo simulations and predictions provided by the standard diffusion approximation [Eqs. (5), (9)–(13) from Ref. [49]] are also plotted. Figures 2(b) and 3(b) provide the error of the δ-P_1 and SDA predictions relative to the MC simulations for both the amplitude and phase, respectively. These figures demonstrate that the δ-P_1 approximation provides a substantial improvement over the SDA in predicting the amplitude and phase of the irradiance at all spatial locations over the full range of optical properties (μ_s'/μ_a). When considering the range of optical properties for which the SDA is expected to perform well $[(\mu_s'/\mu_a)\gtrsim 30]$, we find that the δ-P_1 approximation predictions typically underestimate the amplitude and phase by no more than -18% and -16%, respectively.

Specifically, in Fig. 2 the frequency-domain amplitude predicted by the δ-P_1 approximation approach those given by the SDA in the far-field $(r\gtrsim 5l^*)$. However, in the near-field $(r\lesssim 3l^*)$ we find that the SDA underestimates the measured irradiance by as much 90%; revealing the inability of the SDA to model light fields dominated by unscattered or minimally scattered light. In comparison, the δ-P_1 approximation fares quite well due to its explicit handling of unscattered/ballistic light in both the phase function and ra-

diance approximations. As absorption becomes more significant $[(\mu_s'/\mu_a)\lesssim 10]$, the accuracy of the δ-P_1 amplitude predictions degrade notably and, for $(\mu_s'/\mu_a)=1$, approach -80% error in the far field. However, the accuracy of the δ-P_1 approximation recovers at $(\mu_s'/\mu_a)=0.33$ (data not shown). This improved accuracy for absorption-dominant media is expected because δ-P_1 approximation provides a prediction consistent with Bouguer's law as scattering vanishes [39].

In examining the results shown in Fig. 3, we find that the SDA has great difficulty in modeling the phase delay of the measured irradiance in the near field $(r\lesssim 3l^*)$. By contrast, the δ-P_1 approximation does quite well although it does systematically underestimate the phase by 5–15 %. This error is due to the fact that the δ-P_1 approximation of the single-scattering phase function collapses much of the light that is scattered at small angles into the δ function itself. Thus light that has undergone a number of low angle scattering events, thereby accumulating some phase delay, is modeled by the δ-P_1 approximation as being unscattered without any phase accumulation. We find that this underestimation of phase in the near field persists in the far field. Specifically, although the δ-P_1 predictions for the rate of phase accumulation with radial distance (i.e., $\partial\phi^{ac}/\partial r$) matches the Monte Carlo predictions in the far field, the actual phase delay is underestimated due to the collapse of small angle scattering into the δ function in the near field. These predictions for the phase delay given by the δ-P_1 approximation converge with those given by the SDA in the far field. As the optical absorption increases [i.e., $(\mu_s'/\mu_a)\lesssim 10$], we find that, in contrast to the δ-P_1 frequency-domain amplitude predictions, the accuracy of the phase predictions do not degrade in quality. In fact, the underestimation in the predicted phase delay abates slightly in the near field and translates into a reduction in the percentage error in the far field and the phase appears to be slightly overestimated in the far field for $(\mu_s'/\mu_a)=1$. As with the amplitude predictions, the δ-P_1 predictions for the measured phase consistently outperforms the SDA.

B. Effects of single-scattering asymmetry

An important feature of the δ-P_1 approximation is that the δ-function term in both the phase function and radiance approximations provides the ability to accommodate both the first and second moments of the single-scattering phase function. As a result, unlike the SDA, the δ-P_1 approximation provides radiative transport predictions that depend on the single-scattering asymmetry coefficient g. Figures 4 and 5 provide the spatial distribution of the amplitude and phase of the irradiance for values of g ranging from 0 to 0.95 for a medium with $(\mu_s'/\mu_a)=100$ as determined by both the δ-P_1 and standard diffusion approximations as well as the MC simulations. As before, the source modulation frequency is 100 MHz and the collection fiber possesses $NA=0.37$.

Figure 4 possesses many important features. First, as expected, the SDA provides identical predictions for all values of g because (μ_s'/μ_a) is held fixed. As seen before in Fig. 2 the SDA provides gross underestimates for the frequency-domain amplitude in the near field. However, as the light
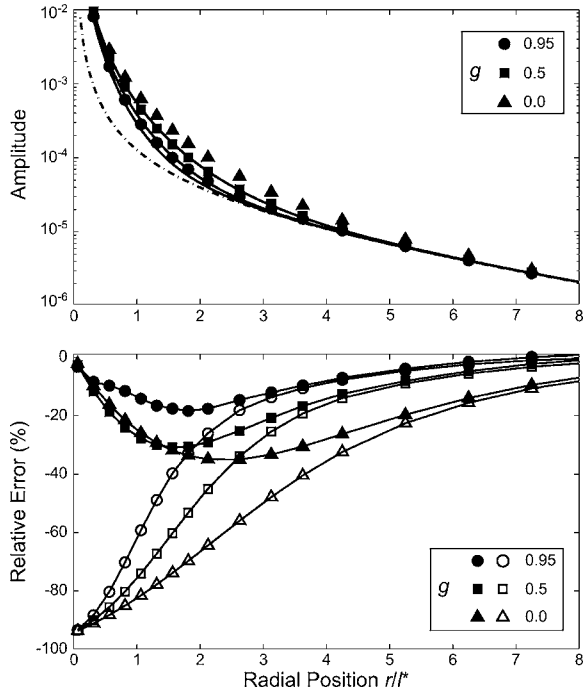
FIG. 4. (a) Photon density wave amplitude vs dimensionless radial position for turbid media with fixed $(\mu_s'/\mu_a)=300$ but varying single-scattering asymmetry of $g=0.95(\bullet)$, 0.5 ($\blacksquare$), and 0.0 ($\blacktriangle$) for source modulation frequency $f=100$ MHz and collection fiber with $NA=0.37$. Monte Carlo estimates are specified by the symbols while predictions by the δ-P_1 and standard diffusion approximation are given by the solid and dashed curves, respectively. (b) Error of the δ-P_1 and standard diffusion approximation predictions relative to the Monte Carlo estimates are specified by the solid and open symbols, respectively.

FIG. 5. (a) Photon density wave phase vs dimensionless radial position for turbid media with fixed $(\mu_s'/\mu_a)=300$ but varying single-scattering asymmetry of $g=0.95(\bullet)$, 0.5 ($\blacksquare$), and 0.0 ($\blacktriangle$) for source modulation frequency $f=100$ MHz and collection fiber with $NA=0.37$. Monte Carlo estimates are specified by the symbols while predictions by the δ-P_1 and standard diffusion approximation are given by the solid and dashed curves, respectively. (b) Error of the δ-P_1 and standard diffusion approximation predictions relative to the Monte Carlo estimates are specified by the solid and open symbols, respectively.

field becomes more diffuse in the far-field, the error of the SDA amplitude predictions vanishes asymptotically. In addition, it is interesting to note that the error in the SDA predictions are lower in magnitude as the value of g increases. This latter feature also holds for the predictions given by the δ-P_1 approximation. This reduced accuracy at lower values of g is attributable to the degradation in the accuracy of δ-P_1 phase function approximation [33]. Conceptually, this can be understood through the fact that as g becomes smaller the need to provide a unscattered component in the phase function subsides and the only improvement offered by the δ-P_1 approximation is the improved description of the photon source [33,38]. Nevertheless, as seen in Fig. 2, the δ-P_1 approximation provides more accurate predictions than the SDA in all the cases considered. Moreover, because we are considering a scattering-dominant medium in Figs. 4 and 5, both δ-P_1 and SDA predictions converge in the far-field.

It is important to note that the amplitude predictions given by the δ-P_1 approximation for the different g values essentially overlap at locations very close to the source ($r \lesssim l^*/2$), "flare" apart at intermediate locations ($l^*/2 \lesssim r \lesssim 3l^*$), and reconverge in the far field ($r \gtrsim 5l^*$). This behavior is also seen in the results of the MC simulation. The first feature arises from the ballistic nature of the radiative transport at locations proximal to the source. As a result, the
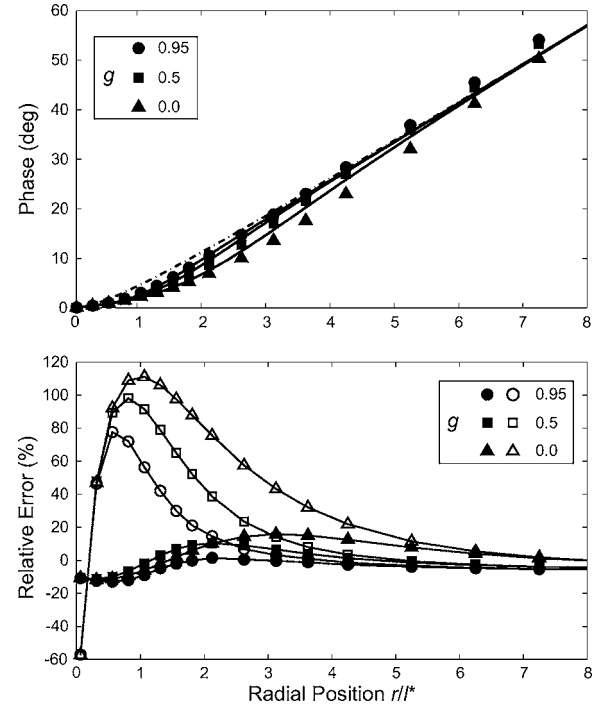
decay in the measured irradiance is dominated by geometric considerations and the details of the light scattering process, as governed by the single-scattering phase function, play a secondary role. However, as the photons propagate further, the character of the light scattering process, specifically the higher order moments of the single scattering phase function, exert an important influence on the spatial decay of the light field. We have termed this region the "transport regime." At locations distal from the source, the light field is dominated by multiply scattered light; conditions under which the similarity conditions for diffusive light transport apply and the characteristics of the light field are sensitive merely to the values of μ_a and μ_s' independent of the moments of the single-scattering phase function [50].

Figure 5 presents results for the spatial variation in the phase of the irradiance and possesses features analogous to those described for Fig. 4. Again, the SDA provides identical predictions for all the g values considered. Also, the accuracy of the estimates provided by both the SDA and δ-P_1 approximation degrade in accuracy for lower values of g. However the error in SDA and δ-P_1 phase predictions vanish asymptotically in the far field. As in Fig. 4, we find that at locations proximal to the source ($r \lesssim l^*$) the phase predictions provided by both the δ-P_1 model and the MC simulations do not show a dependence on g. These predictions "flare" apart at inter-
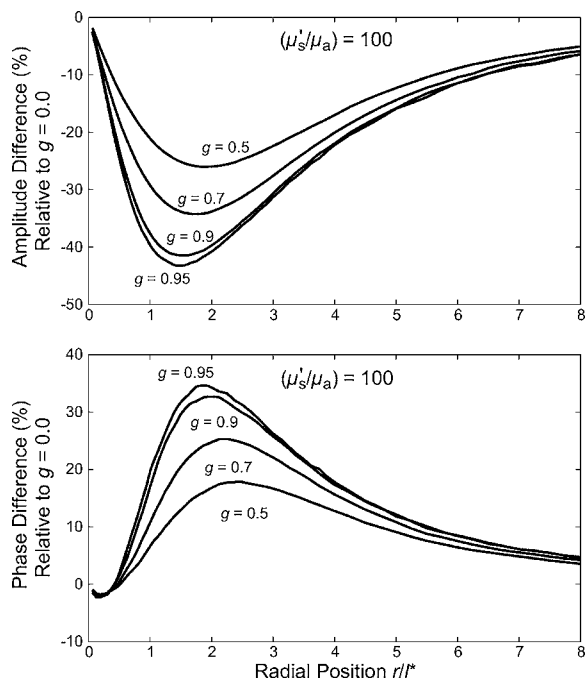
FIG. 6. Difference in photon density (a) amplitude and (b) phase vs dimensionless radial position in asymmetrically scattering media with $g=0.5$, 0.7, 0.9, and 0.95, relative to an isotropically scattering medium. Results are shown within a turbid media with fixed $(\mu_s'/\mu_a)=300$, for a source modulation frequency $f=100$ MHz and collection fiber with $NA=0.37$.
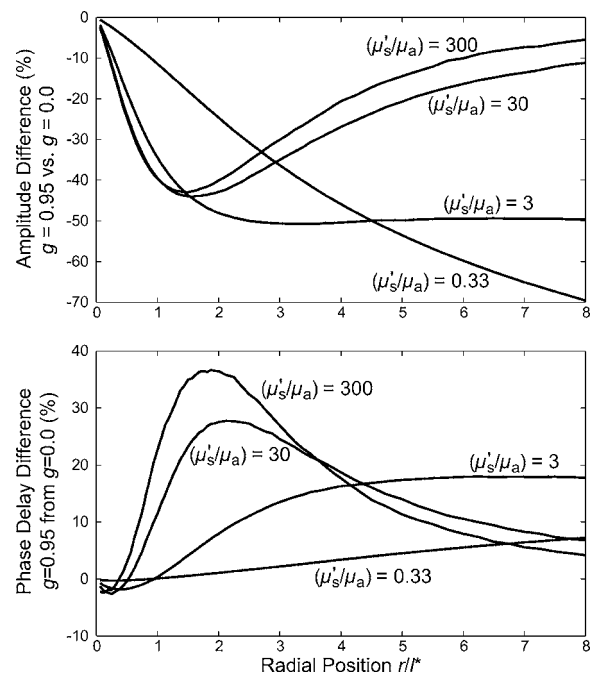
FIG. 7. Difference in photon density (a) amplitude and (b) phase vs dimensionless radial position in a strongly asymmetrically scattering medium ($g=0.95$) relative to an isotropically scattering medium ($g=0$). Results are shown within for turbid media with $(\mu_s'/\mu_a)=300$, 30, 3, and 0.33 for a source modulation frequency $f=100$ MHz and collection fiber with $NA=0.37$.

mediate locations from the source ($l^*\lesssim r\lesssim 5l^*$) and then begin to reconverge in the far-field ($r\gtrsim 6l^*$). This again is due to the evolution of the light field from that dominated by unscattered/ballistic light at locations proximal to the source to that dominated by minimally scattered light at intermediate locations and diffusely scattered light at distal locations. In what follows, these three regimes will be referred to as (a) the ballistic regime, (b) the transport regime, and (c) the diffuse regime.

C. Sensitivity to the scattering asymmetry

The results of Figs. 4 and 5 suggest that a quantitative metric can be developed to identify the spatial locations that represent interfaces between the ballistic, transport, and diffuse regimes. To examine this prospect further, we plot in Fig. 6 the relative (percentage) difference in the frequency domain amplitude [Fig. 6(a)] and phase delay [Fig. 6(b)] of the measured irradiance between a medium that highly forward scatters light ($g>0$) vs a medium that displays isotropic scattering ($g=0$). This result for a medium with $(\mu_s'/\mu_a)=100$ and illuminated by an intensity modulated source at 100 MHz is plotted for values of the single-scattering asymmetry coefficient spanning $0.5\leq g\leq 0.95$. These plots show that light transport is not sensitive to the single-scattering asymmetry at locations very close ($r\lesssim 0.5l^*$) or very far from the source ($r\gtrsim 5l^*$). As noted previously, this is due to the fact that locations proximal to the source lie in the ballistic regime where the light transport is

dominated by geometrical considerations and insensitive to the single-scattering phase function. On the other hand, locations distal from the source lie in the diffuse regime where multiple light scattering dominate the propagation and the similarity relations apply. However for intermediate locations, i.e., in the transport regime, we see that the light propagation is affected significantly by the single-scattering asymmetry. Specifically, for a fixed (μ_s'/μ_a), increases in the single-scattering asymmetry result in a decrease in amplitude and an increase in phase delay. This occurs because for a fixed (μ_s'/μ_a) an increase in single-scattering asymmetry g is coupled with an increase in the scattering coefficient. Thus when considering light propagation over a distance larger than a transport mean free path, the photon traveling in a medium with large g will experience many closely spaced forward-directed scattering events whereas a photon traveling in an isotropically scattering medium will experience fewer, but isotropic, scattering events. This larger number of scattering events results in both an increased phase delay and greater attenuation in media with large g. For a medium of $(\mu_s'/\mu_a)=100$ the sensitivity to the single-scattering asymmetry is most prominent at radial locations $0.5l^*\gtrsim r\gtrsim 5l^*$ and is the principal characteristic of the transport regime.

To examine how the spatial location of the ballistic, transport, and diffuse regimes are affected by the optical properties of the medium, in Fig. 7 we plot the relative difference in the frequency domain amplitude [Fig. 7(a)] and phase [Fig. 7(b)] of the measured irradiance between a highly forward scattering medium ($g=0.95$) and isotropically scattering medium ($g=0$) for media of $300\geq(\mu_s'/\mu_a)\geq 0.33$. For highly

scattering media [i.e., $(\mu_s'/\mu_a) \gtrsim 10$] we find that the features of both the amplitude and phase plots are similar to those shown in Fig. 6. Specifically, we can clearly identify a ballistic regime at locations proximal to the source and a diffuse regime at locations distal from the source. However, for lower values of (μ_s'/μ_a), the spatial region in which radiative transport predictions are sensitive to the value of g gets larger. As a result the domain in which the frequency-domain amplitude and phase are not affected by the single-scattering asymmetry, i.e., the diffuse regime, is displaced to radial locations further away from the source. Interestingly for values of $(\mu_s'/\mu_a) \lesssim 10$ we find that beyond the ballistic regime at radial locations proximal to the source, the differences in the radiative transport due to the different values of the single-scattering asymmetry are permanent. Thus it appears that a diffuse regime, as defined by distal radial locations where the scattering asymmetry does not produce significant differences in either the measured amplitude or phase, does not exist. This occurs because in media of moderate and high absorption, photons are absorbed at such a rate that even in the presence of scattering, a quasi-isotropic light field is not achievable at locations far from the source. This is consistent with the fact that radiative transport predictions provided by the SDA are not accurate for media of $(\mu_s'/\mu_a) \lesssim 10$ even at locations far from a light source. This can be expected especially when one remembers that in the limit $(\mu_s'/\mu_a) \rightarrow 0$, light transport is solely ballistic and neither a transport nor a diffuse regime exists.

These plots permit an objective definition for the location of the transport regime which we will specify as those radial locations where the frequency-domain amplitude or phase in a medium with $g = 0.95$ differs from that in a medium with $g = 0$ by more than $\pm 10\%$. While the specific choice of 10% is arbitrary, it provides an objective criterion by which we can define the limits of the ballistic, transport, and diffuse regimes. Note that with this definition, the interfaces demarcating the boundaries of these regimes may reside at different locations depending on whether one considers the frequency-domain amplitude or phase of the irradiance. This provides for the examination of two interfaces: that between the ballistic and transport regimes $r_{B \rightarrow T}$ and that between the transport and diffuse regimes $r_{T \rightarrow D}$. As can be readily appreciated from the results shown in Fig. 7, both $r_{B \rightarrow T}$ and $r_{T \rightarrow D}$ are affected by (μ_s'/μ_a). However, apart from optical properties, these interface locations are sensitive to both the numerical aperture of the collection fiber [39] and the source modulation frequency [51].

In Figs. 8 and 9, we plot the locations of these two interfaces as a function of (μ_s'/μ_a) for various numerical apertures and source modulation frequencies, respectively. In Figs. 8(a) and 9(a), the interfaces are based on the amplitude of the frequency-domain irradiance whereas in Figs. 8(b) and 9(b) the interfaces are based on the phase of the frequency-domain irradiance. Both Figs. 8 and 9 show that both interfaces move closer to the source for increasing values of (μ_s'/μ_a) when considering either the frequency domain amplitude or phase delay. This indicates that increases in optical scattering reduce the contribution of unscattered light to the total light field at large distances. Put another way, in the
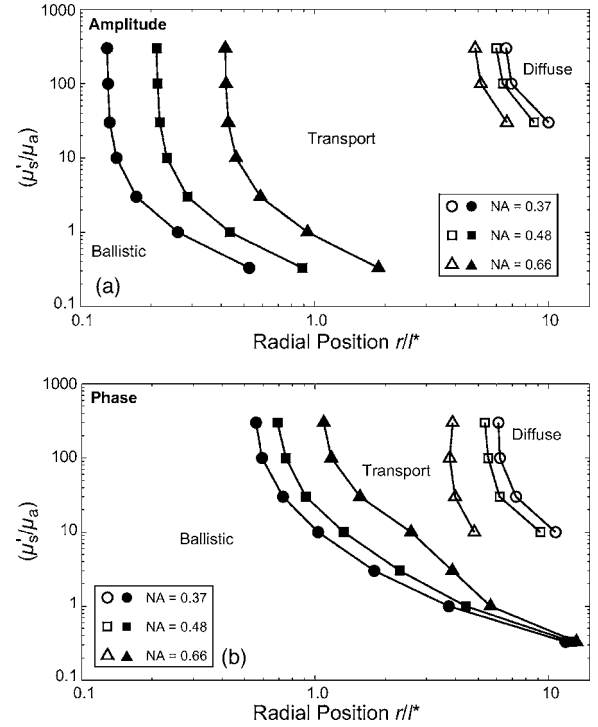

FIG. 8. Variation of the positions of the interfaces separating the ballistic and transport regions $r_{B \rightarrow T}$ and the transport and diffuse regions $r_{T \rightarrow D}$ as determined by differences in frequency-domain (a) amplitude and (b) phase delay. Variation of the interface locations with optical properties (μ_s'/μ_a) and numerical aperture of the detection fiber *NA* are provided as indicated. Source modulation frequency is fixed at $f = 100$ MHz.

limit for which scattering is absent, i.e., $(\mu_s'/\mu_a) \rightarrow 0$, the light field is ballistic throughout and $r_{B \rightarrow T} \rightarrow \infty$.

Comparison of Figs. 8(a) and 8(b) shows that transition from the ballistic to transport regime $r_{B \rightarrow T}$, based on phase delay differences occur at locations further from the source than those based on amplitude. This interface represents a transition from a light field dominated by ballistic light to that dominated by multiply scattered light. Thus a comparison of these figures indicates that while multiple scattering leads to differences in the measured amplitude based on the value of the single-scattering asymmetry coefficient at locations fairly proximal to the source, many more scattering events are required to result in a significant difference in the phase delay. As such, the transition from the ballistic to transport regime occurs further away from the source for the phase delay of the measured frequency-domain irradiance as opposed to the amplitude. We see that a decrease of numerical aperture results in the movement of $r_{B \rightarrow T}$ toward the source. This is expected because a reduction of numerical aperture reduces the probability that singly scattered photons will be detected. Thus their "absence" from the irradiance will be detected at distances closer to the source.

When considering the transition from the transport to diffuse regime as shown in Figs. 8(a) and 8(b), we find that the location of this interface is much less sensitive to the type of measurement (amplitude or phase) that one considers. This implies that the insensitivity of a frequency-domain ampli-
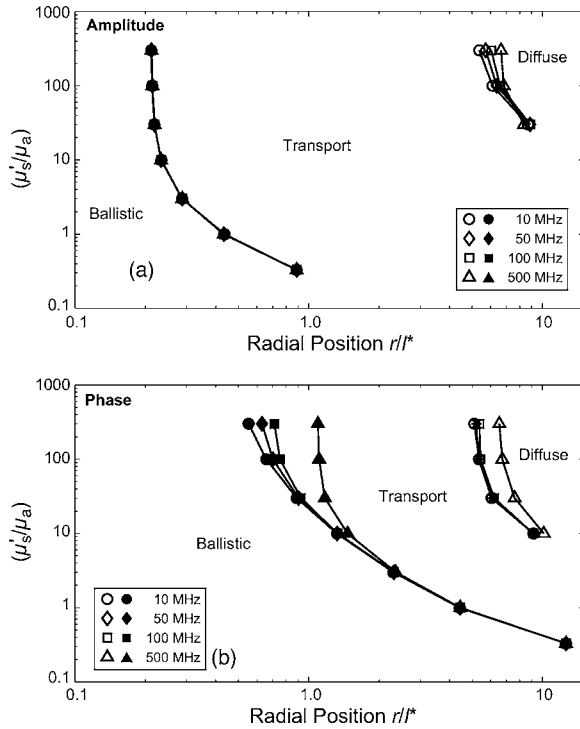
FIG. 9. Variation of the positions of the interfaces separating the ballistic and transport regions $r_{B \to T}$ and the transport and diffuse regions $r_{T \to D}$ as determined by by differences in frequency-domain (a) amplitude and (b) phase delay. Variation of the interface locations with optical properties (μ_s'/μ_a) and source modulation frequency f are provided as indicated. The numerical aperture of the collection fiber is fixed at $NA = 0.37$.

tude or phase delay measurement to the single-scattering asymmetry of the medium occurs at roughly the same location. However, the results do show that for a given set of optical properties $r_{T \to D}$ tends to be slightly larger for the amplitude as compared to phase delay. This implies that the impact of the single-scattering asymmetry on radiative transport is "communicated" to slightly deeper regions of the turbid medium when considering the amplitude as opposed to the phase of the irradiance. This finding is consistent with earlier studies examining the spatial sampling of photon density waves that report the phase component of the measured frequency-domain irradiance to be sensitive to slightly deeper regions in turbid media than the amplitude [51–53]. We also find that a decrease in (μ_s'/μ_a) and/or numerical aperture results in a displacement of the $r_{T \to D}$ interface to deeper positions in the turbid medium. Both these characteristics are expected as a reduction in scattering requires a longer path length in order for the light field to become randomized and a smaller collection angle will increase the sensitivity of the collection fiber to the presence of ballistic and minimally scattered photons.

In Fig. 9 we plot the locations of these interfaces as a function of (μ_s'/μ_a) for various source modulation frequencies as shown in Fig. 9(a) for the frequency-domain amplitude and Fig. 9(b) for the frequency-domain phase delay. These results are generally consistent with earlier work from our group demonstrating that the sampling volume of

frequency-domain diffuse reflectance can be modified by the source modulation frequency [51]. This dependence on source modulation frequency can be attributed to the changes in temporal windowing of the detected irradiance. These plots display three notable features. First, increases in (μ_s'/μ_a) result in the movement of both interfaces closer to the source. Second, reductions in (μ_s'/μ_a) reduce the sensitivity of the interface locations to the source modulation frequency. Third, for highly scattering media, reductions in modulation frequency result in the movement of both $r_{B \to T}$ and $r_{T \to D}$ closer to the source.

The movement of both $r_{B \to T}$ and $r_{T \to D}$ closer to the source with increasing (μ_s'/μ_a) is due to the increased probability of scattering relative to absorption that hastens the transition of the ballistic light to the transport and diffuse regimes [49,54]. The second and third characteristics are consistent with the propagation characteristics of photon density waves. The propagation of photon density waves is characterized by linear and dispersive regimes. The linear regime is dominant when the source modulation frequency f_{mod} is much smaller that the reciprocal absorption relaxation time $1/\tau_a$ which we shall call the absorption relaxation frequency $f_a = \tau_a^{-1} = \mu_a v/2\pi$. In the linear regime, the propagation and attenuation characteristics of the photon density wave are independent of the source modulation frequency [54]. If we consider the medium under question to have a fixed $\mu_s' = 1$ mm^{-1}, f_a varies from 3 GHz for a medium with $(\mu_s'/\mu_a) = 10$ to 100 MHz for a medium with $(\mu_s'/\mu_a) = 300$. Thus as we consider more highly scattering media we begin to probe a regime where the photon density wave propagation becomes dispersive. In the dispersion regime both the phase velocity and attenuation of the photon density wave increase with modulation frequency [54]. As a result for media with $(\mu_s'/\mu_a) \gtrsim 100$ the consideration of modulation frequencies in the range of 10–500 MHz, effectively probes the transition between the linear and dispersive regimes. Specifically, we find that both $r_{B \to T}$ and $r_{T \to D}$ increase with modulation frequency. The displacement of these interfaces to locations further from the source is representative of the increase in phase velocity of photon density waves with increasing modulation frequency in the dispersion regime. As a result, higher frequency photon density waves undergo less scattering and must propagate further before making the transition into the transport and ultimately the diffuse regime. Thus for a given distance from a photon source both reductions in numerical aperture and increases in source modulation frequency can provide more sensitivity to the ballistic and transport components of the overall light field.

V. SUMMARY AND CONCLUSIONS

In this study, we have demonstrated the use of the δ-P_1 approximation to characterize the propagation of photon density waves under conditions where the angular distribution of the light field is highly asymmetric, namely, at locations proximal to light sources and in highly absorbing media. Comparison of δ-P_1 estimates for both amplitude and phase components of the frequency domain irradiance were compared to the results of Monte Carlo simulations and the stan-

dard diffusion approximation. In all cases, predictions provided by the δ-P_1 approximation outperform those given by the standard diffusion approximation. Of particular note is the ability of the δ-P_1 approximation to provide excellent phase delay predictions over a wide range of source-detector separation and (μ_s'/μ_a).

These improved estimates are achieved by adding unscattered/ballistic components to both scattering phase function and radiance approximations. The δ-P_1 phase function provides a description of the highly asymmetric nature of light scattering. The addition of the δ component to the phase function approximation models more effectively the asymmetric nature of light scattering by shifting the probability of small scattering angles to the forward peak. Separation of the radiance into ballistic and diffuse components allows the δ-P_1 approximation to accurately model both the spatial distribution and temporal characteristics of directed light sources. Thus the δ-P_1 approximation provides improvements in three aspects of the light transport modeling by providing a higher-order radiance/phase function approximation, accurately modeling directed light sources and accounting for the time-of-flight of ballistic photons emitted by the source.

The higher-order phase function approximation used in the δ-P_1 approximation provides radiative transport estimates that vary with the single-scattering asymmetry g independently from the reduced scattering coefficient μ_s'. This prompted an examination of the spatial regions in which the measured frequency domain amplitude and phase delay are sensitive to g for fixed values of (μ_s'/μ_a). This provided a framework to divide the spatial domain into three regimes: ballistic, transport, and diffuse. Unscattered and diffusely scattered light dominate the light field in the ballistic and diffuse regimes, respectively, and thus display minimal dependence on g. The light field in the transport regime is multiply scattered but shows a strong sensitivity to g and represents the transition from ballistic to diffuse light transport. Our results show that the spatial location of these regimes depends not only on the optical properties of the medium but also upon the source modulation frequency and numerical aperture of detection.

ACKNOWLEDGMENTS

[1] D. A. Boas, M. A. O'Leary, B. Chance, and A. G. Yodh, Appl. Opt. **36**, 75 (1997).

[2] A. E. Cerussi, D. Jakubowski, N. Shah, F. Bevilacqua, R. Lanning, A. J. Berger, D. Hsiang, J. Butler, R. F. Holcombe, and B. J. Tromberg, J. Biomed. Opt. **7**, 60 (2002).

[3] D. T. Delpy and M. Cope, Philos. Trans. R. Soc. London, Ser. B **352**, 649 (1997).

[4] T. J. Farrell, M. S. Patterson, and B. Wilson, Med. Phys. **19**, 879 (1992).

[5] M. A. Franceschini, E. Gratton, and S. Fantini, Opt. Lett. **24**, 829 (1999).

[6] A. Kienle and M. S. Patterson, J. Opt. Soc. Am. A **14**, 246 (1997).

[7] T. O. McBride, B. W. Pogue, S. Poplack, S. Soho, W. A. Wells, S. Jiang, U. L. Österberg, and K. D. Paulsen, J. Biomed. Opt. **7**, 72 (2002).

[8] W. M. Star, Phys. Med. Biol. **42**, 763 (1997).

[9] A. Li, Q. Zhang, J. P. Culver, E. L. Miller, and D. A. Boas, Opt. Lett. **29**, 256 (2004).

[10] A. Corlu, T. Durduran, R. Choe, M. Schweiger, E. M. C. Hillman, S. R. Arridge, and A. G. Yodh, Opt. Lett. **28**, 2339 (2003).

[11] N. Shah, A. Cerussi, C. Eker, J. Espinoza, J. Butler, J. Fishkin, R. Hornung, and B. Tromberg, Proc. Natl. Acad. Sci. U.S.A. **98**, 4420 (2001).

[12] B. J. Tromberg, N. Shah, R. Lanning, A. Cerussi, J. Espinoza, T. Pham, L. Svaasand, and J. Butler, Neoplasia **2**, 26 (2000).

[13] J. J. Duderstadt and W. R. Martin, *Transport Theory* (Wiley, New York, 1979).

[14] A. Ishimaru, *Wave Propagation and Scattering in Random Media* (Academic, New York, 1978), Vols. 1&2.

[15] T. J. Farrell and M. S. Patterson, J. Biomed. Opt. **6**, 468 (2001).

[16] J. B. Fishkin, S. Fantini, M. J. vandeVen, and E. Gratton, Phys. Rev. E **53**, 2307 (1996).

[17] L. V. Wang and S. L. Jacques, Comput. Methods Programs Biomed. **61**, 163 (2000).

[18] A. Amelink, H. J. C. M. Sterenborg, M. P. L. Bard, and S. A. Burgers, Opt. Lett. **29**, 1087 (2004).

[19] L. Nieman, A. Myakov, J. Aaron, and K. Sokolov, Appl. Opt. **43**, 1308 (2004).

[20] M. Canpolat and J. R. Mourant, Appl. Opt. **40**, 3792 (2001).

[21] F. Bevilacqua and C. Depeursinge, J. Opt. Soc. Am. A **16**, 1935 (1999).

[22] I. Charvet, P. Theuler, B. Vermeulen, M. Saint-Ghislain, C. Biton, J. Jacquet, F. Bevilacqua, C. Depeursinge, and P. Meda, Phys. Med. Biol. **47**, 2095 (2002).

[23] A. K. Dunn, A. Devor, H. Bolay, M. L. Andermann, M. A. Moskowitz, A. M. Dale, and D. A. Boas, Opt. Lett. **28**, 28 (2003).

[24] E. M. C. Hillman, D. A. Boas, A. M. Dale, and A. K. Dunn, Opt. Lett. **29**, 1650 (2004).

[25] P. Thueler, I. Charvet, F. Bevilacqua, M. St. Ghislain, G. Ory, P. Marquet, P. Meda, B. Vermeulen, and C. Depeursinge, J. Biomed. Opt. **8**, 495 (2003).

[26] K. M. Case and P. F. Zweifel, *Linear Transport Theory* (Addison-Wesley Publishing Co., Reading, MA, 1967).

[27] D. Dickey, O. Barajas, K. Brown, J. Tulip, and R. B. Moore, Phys. Med. Biol. **43**, 3559 (1998).

[28] D. Dickey, R. B. Moore, D. C. Rayner, and J. Tulip, Phys. Med. Biol. **46**, 2359 (2001).

[29] E. L. Hull and T. H. Foster, J. Opt. Soc. Am. A **18**, 584 (2001).

[30] J. C. Finlay and T. H. Foster, Med. Phys. **31**, 1949 (2004).

[31] D. A. Boas, H. Liu, M. A. O'Leary, B. Chance, and A. G. Yodh, Proc. SPIE **2389**, 240 (1995).

[32] S. Fantini, M. A. Franceschini, and E. Gratton, Appl. Opt. **36**, 156 (1997).

[33] J. H. Joseph, W. J. Wiscombe, and J. A. Weinman, J. Atmos. Sci. **33**, 2452 (1976).

[34] S. A. Prahl, Ph.D. thesis, University of Texas at Austin, 1988.

[35] W. M. Star, J. P. A. Marijnissen, and M. J. C. van Gemert, Phys. Med. Biol. **33**, 437 (1988).

[36] W. M. Star, in *Dosimetry of Laser Radiation in Medicine and Biology*, edited by G. J. Müller and D. H. Sliney (SPIE, Bellingham, WA, 1989), pp. 146–154.

[37] T. Spott and L. O. Svassand, Appl. Opt. **39**, 6453 (2000).

[38] S. A. Carp, S. A. Prahl, and V. Venugopalan, J. Biomed. Opt. **9**, 632 (2004).

[39] V. Venugopalan, J. S. You, and B. J. Tromberg, Phys. Rev. E **58**, 2395 (1998).

[40] C. K. Hayakawa, B. Y. Hill, J. S. You, F. Bevilacqua, J. Spanier, and V. Venugopalan, Appl. Opt. **43**, 4677 (2004).

[41] D. J. Durian and J. Rudnick, J. Opt. Soc. Am. A **14**, 235 (1997).

[42] P.-A. Lemieux, M. U. Vera, and D. J. Durian, Phys. Rev. E **57**, 4498 (1998).

[43] S. L. Jacques, C. A. Alter, and S. A. Prahl, Lasers Life Sci. **1**, 309 (1987).

[44] W. M. Star, in *Optical-Thermal Response of Laser-Irradiated Tissue*, edited by A. J. Welch and M. J. C. van Gemert (Plenum, New York, 1995), pp. 131–206.

[45] A. Dunn and C. DiMarzio, J. Opt. Soc. Am. A **14**, 65 (1996).

[46] L. G. Henyey and J. L. Greenstein, Astrophys. J. **93**, 70 (1941).

[47] J. Spanier and E. M. Gelbard, *Monte Carlo Principles and Neutron Transport Problems* (Addison-Wesley, Reading, MA, 1969).

[48] M. Testorf, U. Osterberg, B. Pogue, and K. Paulsen, Appl. Opt. **38**, 236 (1999).

[49] B. J. Tromberg, L. O. Svaasand, T-T. Tsay, and R. C. Haskell, Appl. Opt. **32**, 607 (1993).

[50] D. R. Wyman, M. S. Patterson, and B. C. Wilson, Appl. Opt. **28**, 5243 (1989).

[51] F. Bevilacqua, J. S. You, C. K. Hayakawa, and V. Venugopalan, Phys. Rev. E **69**, 051908 (2004).

[52] G. Gratton, J. S. Maier, M. Fabiani, W. W. Mantulin, and E. Gratton, Psychophysiology **31**, 211 (1994).

[53] E. M. Sevick, J. K. Frisoli, C. L. Burch, and J. R. Lakowicz, Appl. Opt. **33**, 3562 (1994).

[54] L. O. Svaasand, B. J. Tromberg, R. C. Haskell, T.-T. Tsay, and M. W. Berns, Opt. Eng. (Bellingham) **32**, 258 (1993).